Available online at www.sciencedirect.com
SCIENCE DIRECT®
Computer Coupling of Phase Diagrams and Thermochemistry 29 (2005) 24–36
www.elsevier.com/locate/calphad

Thermodynamic modeling of the Mg–Al–Sb system

T. Balakumar, M. Medraj*

Department of Mechanical and Industrial Engineering, Concordia University, 1455 de Maisonneuve Blvd. West, H-549, Montreal, Quebec, H3G 1M8, Canada

Received 30 December 2004; received in revised form 24 February 2005; accepted 4 March 2005
Available online 7 April 2005

Abstract

Thermodynamic modeling of the Mg–Al–Sb system is carried out for the first time in this work. Among the constituent binaries in this system, only the Al–Sb and Mg–Sb are re-optimized. Liquid phases are described by the Redlich–Kister polynomial model, whereas the high temperature modification of Mg_3Sb_2 compound in the Mg–Sb system is described by the sublattice model. The constructed database is used to calculate and predict thermodynamic properties, binary phase diagrams of Al–Sb and Mg–Sb, and liquidus projections of the ternary Mg–Al–Sb. The calculated phase diagrams and the thermodynamic properties such as enthalpy, entropy, Gibbs free energy of mixing, and activities are found to be in good agreement with the experimental data from the literature. The established Mg–Al–Sb database predicted a closed ternary liquid miscibility gap, six ternary eutectics, two ternary peritectics, four saddle points and a critical point.

Keywords: Thermodynamic modeling; Al–Sb system; Mg–Sb system; Mg–Al–Sb system; Liquid miscibility gap; Mg–Al based alloys

1. Introduction

The current need for higher fuel-efficient vehicles increases the demand for magnesium alloys due to their light weight and good specific mechanical properties. However, the use of magnesium alloys has been limited due to their poor creep resistance. Hence, new magnesium alloys are needed to meet the automobile and aerospace requirements for elevated temperature strength.

Approximately 90% of all magnesium cast products are being made out of the standard magnesium die-casting alloy AZ91 (Mg–9.2Al–0.88Zn–0.34Mn) [1]. This magnesium alloy has excellent castability and in its high purity form (AZ91E) shows good corrosion resistance. However, it suffers from low creep resistance at temperatures in excess of 393 K which makes it unsuitable for many of the components in automobile engines [1]. For components used in automotive or aerospace applications, the most important type of creep is high temperature creep. It is found that, in the specific case of magnesium and its alloys, grain boundary sliding makes the major contribution to creep strain [2–4]. The resistance to grain boundary sliding can be improved by producing thermally stable grain boundary phase. It is found that a small amount of Sb additions to AZ91 based alloys significantly increases the yield strength and creep resistance at elevated temperature up to 473 K [5]. Moreover, the work of Guangyin et al. [5] indicated that the addition of Sb causes the formation of some rod-shaped precipitates of Mg_3Sb_2 with hexagonal $D5_2$ structure which strengthen both matrix and grain boundaries effectively. They also observed fine precipitates of Mg_3Sb_2 in the alloy Mg–9Al–0.8Zn–0.2Mn–0.35Sb, even after 50 h of creep at 473 K and 50 MPa. Hence these precipitates are thermally stable. Therefore, studying the Mg–Al–Sb system is important for understanding and developing creep resistant magnesium alloys in this system.

The constituent binaries in the Mg–Al–Sb system are: Mg–Al, Al–Sb, and Mg–Sb. The Al–Sb system exhibits a simple phase diagram with two eutectic points and an intermediate line compound AlSb. There is no evidence in the literature for mutual solubility between Al and Sb. The different phases in this system are: Al-fcc, Sb-rhombo, AlSb,

* Corresponding author. Tel.: +1 514 848 2424x3146; fax: +1 514 848 3175.
E-mail address: mmedraj@encs.concordia.ca (M. Medraj).

0364-5916/$ - see front matter © 2005 Elsevier Ltd. All rights reserved.
doi:10.1016/j.calphad.2005.03.001

and liquid. There are three invariant reactions in this system: one on the Al-rich side, L → Al-fcc + AlSb, another on Sb-rich side, L → AlSb + Sb-rhombo, and the third at $X_{Sb} = 0.5$, L → AlSb.

Different phases in the Mg–Sb system are: liquid, Mg-hcp, Sb-rhombo, and intermediate compound Mg_3Sb_2. The intermediate compound has two crystalline modifications. The low temperature modification, α-Mg_3Sb_2, is treated as a stoichiometric compound. But the high temperature modification β-Mg_3Sb_2 is a non-stoichiometric compound with a narrow range of composition towards the Mg-rich side. In this case, there is no evidence available on the types of defects which make the deviation from stoichiometry. Furthermore, it is assumed that there is no solubility between Mg and Sb in this system. Due to the unusual liquidus shape of the β-Mg_3Sb_2, it is extremely difficult to get the optimized model parameters. There are two eutectic points observed. One is on the Mg-rich side, and occurs according to L → Mg-hcp + α-Mg_3Sb_2. The second eutectic is on the Sb-rich side, and occurs according to L → Sb-rhombo + α-Mg_3Sb_2.

The Mg–Al system has two terminal solid solutions, namely Mg-hcp and Al-fcc. This binary system has two line compounds, $Al_{30}Mg_{23}$ and $Al_{140}Mg_{89}$, and a non-stoichiometric compound Gamma (γ). The line compound $Al_{30}Mg_{23}$ is stable only in the temperature range 523–683 K. There are four invariant reactions in this system: eutectic reactions on the Mg-rich side, L → Mg-hcp + γ, between γ and $Al_{140}Mg_{89}$, L → γ + $Al_{140}Mg_{89}$ and on the Al-rich side, L → $Al_{140}Mg_{89}$ + fcc-Al. The congruent melting reactions are at $X_{Al} = 0.463$, $T = 737$ K: L → γ and at $X_{Al} = 0.611$, $T = 725$ K: L → $Al_{140}Mg_{89}$.

The Mg–Al–Sb ternary has not been investigated completely. Guertler and Bergman [6,7], and Loofs-Rassow [8] carried out microscopical and thermal examinations on the Al–Sb–Mg system. Guertler and Bergman [7] performed thermal analysis on the quasi-binary Al–Mg_3Sb_2. For the Mg–Al–Sb system, neither ternary compound nor thermodynamic data were reported in the literature.

2. Data analysis

The accuracy of the thermodynamic model of a system depends on the reliability of the data used in the thermodynamic model parameters' optimization. Hence, it is important to select reliable experimental data from the literature for this purpose. The following sections analyze the previous research work on Al–Sb, Mg–Sb, Mg–Al, and Mg–Al–Sb systems, show how reliable data are extracted from a pool of available data and derive the aim of the present research.

2.1. Al–Sb binary system

2.1.1. Phase diagram data

The latest assessment of the Al–Sb system was carried out by Yamaguchi et al. [9]; they used an associated solution model to describe the liquid phase. Coughanowr et al. [10] have reviewed the previous works on the Al–Sb system and carried out an assessment on thermodynamic properties and phase diagram data using the Lukas optimization program. They used the Redlich–Kister and associated solution model separately and compared the optimized results. The two models showed a slight difference in the temperatures of the Al-rich eutectic line and of the congruent melting of AlSb. Later Yamaguchi et al. [11] measured the heat content of Al–Sb alloys using a drop calorimeter in a temperature range 800–1450 K and in a concentration range $0.05 \leq X_{Sb} \leq 0.95$, and determined the Al–Sb phase diagram from the heat content–temperature–composition relationships. Moreover, they measured the heat and entropy of formation of AlSb using a twin solution calorimeter and an adiabatic calorimeter respectively and calculated the Al–Sb system using the Redlich–Kister polynomial model. Their calculated phase diagram was found to be in good agreement with their experimental work as well as with other experimental data reported in the literature. Especially, the liquidus line of the Al-rich side agrees with Guertler and Bergmann [6] and the Sb-rich side agrees with Linnebach and Benz [12].

Among the available optimized model parameters for the Al–Sb system Yamaguchi et al. [9] used the associated solution model to describe the liquid phase. As the present research is a part of a multicomponent database for Mg alloys that describes the liquid by the Redlich–Kister polynomial model, their parameters cannot be used in conjunction with other subsystems. Another work by Yamaguchi et al. [11] provided the parameters for the liquid Al–Sb by the Redlich–Kister polynomial model. However, they used too many parameters (12 parameters) to describe the liquid phase. As a simpler model was found to provide the clearest insight into the basic properties of the system [13], this system is re-optimized with the aim of finding fewer model parameters to describe this system.

Zajaczkowski and Botor [14] also studied the Al–Sb system using vapor pressure measurements, calculated the system using a regular associate solution model, and determined the Al–Sb phase diagram. The invariant points reported in Yamaguchi et al. [11] and Zajaczkowski and Botor [14] showed slight differences in temperature and composition. From the above mentioned data analysis, the present work adopts the liquidus points reported in Yamaguchi et al. [11]. Further, Lichter and Sommelet [15] measured the high temperature heat content and heat of fusion of AlSb, and determined the melting point of AlSb as 1330 ± 5 K. The results obtained in the current research are compared with their findings.

2.1.2. Thermodynamic data

The Al–Sb system is found to be less investigated with regard to experimental determination of its thermodynamic properties. There are only scarce literature data available on the enthalpy and Gibbs free energy of the liquid phase of

this system. Yamaguchi et al. [11] derived the integral molar quantities of the liquid Al–Sb alloys from the heat content for the Al–Sb system and the heat and entropy of formation of the AlSb compound which were obtained by calorimetric measurements. They conducted their experiments using different mole fractions of Sb in the range $0.05 \leq X_{Sb} \leq 0.95$ within the temperature range 800–1450 K. Previously Girard et al. [16] measured the enthalpy of mixing values for the liquid Al–Sb alloys in the temperature range 968–1227 K by a drop calorimeter method using a Calvet micro calorimeter. However, they did not cover the complete composition range, and they reported the enthalpy of liquid Al–Sb in the composition ranges $0 < X_{Sb} < 0.2$ and $0.7 < X_{Sb} < 1.0$. On the Al-rich side, the reported enthalpy of mixing values of Girard et al. [16] showed very big deviation from those of Yamaguchi et al. [11]. On the other hand, their values show fairly good agreement on the Sb-rich side. Another work by Batalin et al. [17] on the enthalpy of mixing of liquid Al–Sb alloy measurement shows complete disagreement with other authors' measurements. The Gibbs free energy of mixing and the entropy of mixing values for liquid Al–Sb alloys were only reported by Yamaguchi et al. [11] at 1350 K. There are very few measurements reported in the literature on the thermodynamic activities of Al and Sb in liquid Al–Sb alloys. Zajaczkowski and Botor [14] determined the thermodynamic activity of Al and Sb by measuring the vapor pressure of Sb in liquid Al–Sb alloys in the composition range $0.0264 \leq X_{Sb} \leq 0.9858$ and in the temperature range 950–1461 K. Predel and Schallner [18] also studied the thermodynamic activities of Al and Sb in liquid Al–Sb alloys. From the above thermodynamic data analysis, it can be seen that the thermodynamic properties reported by Yamaguchi et al. [11] and Zajaczkowski and Botor [14] are the more recent and reliable values. Hence, the present work considers their data in the thermodynamic model parameter optimization.

2.2. Mg–Sb binary system

2.2.1. Phase diagram data

The work on Mg–Sb phase diagram development was first started in 1906 by Grube [19], when he determined the liquidus temperature across the whole concentration range. However, the reported liquidus values were found to be unreliable and they were re-determined later in 1934 by Grube himself and Bornhak [20] using thermal analysis. Moreover, Jones and Powell [21] performed thermal analysis on the Mg-rich side, in the composition range $0 \leq X_{Sb} \leq 0.014$, and determined the liquidus line. Later on, Hansen and Anderko [22] reported the liquidus points of Mg–Sb system for the complete composition range. Also, this system was assessed by Nayeb-Hashemi and Clark [23], and Jönsson and Ågren [24].

Since the work of Nayeb-Hashemi and Clark [23] is more recent than the other works, the present research considers their results for the liquidus points in this system. Zabdyr and Moser [25] investigated dilute solutions of Mg in the Mg–Sb system using an emf technique and calculated part of the liquidus in the Sb-rich side of the Mg–Sb phase diagram. Rao and Patil [26] also reported liquidus points for the Sb-rich side. Their reported values are found to be in good agreement with Zabdyr and Moser [25]. For this system, only Jönsson and Ågren [24] provided the optimized model parameters. They used an associated solution model to describe the liquid phase. Since the present research uses the Redlich–Kister polynomial model to describe the liquid phase in Mg base alloys, the parameters of [24] cannot be used and the Mg–Sb system was re-optimized.

The melting point of the β-Mg_3Sb_2 phase was re-determined by Bolshakov et al. [27] using differential thermal analysis (DTA) measurements as 1518 ± 5 K. This value is 17 K higher than that of both Grube and Bornhak [20], and Hansen and Anderko [23]. Bolshakov et al. [27] reported the transformation temperature of the α-Mg_3Sb_2 to β-Mg_3Sb_2 as 1198 ± 5 K. The upper limit of this value is in accord with the value reported by Grube and Bornhak [20]. On the other hand, only Jones and Powell [21] reported a very small solubility of Sb in Mg. Hence, the present work is carried out by assuming no mutual solubility between Mg and Sb.

2.2.2. Thermodynamic data

The thermodynamic properties of Mg in liquid Mg–Sb alloys such as activities, relative partial molar free energies, entropies and enthalpies were determined by Rao and Patil [26] using emf measurements. They determined these thermodynamic properties in the temperature range 980–1250 K and in the composition range $0.4 \leq X_{Sb} \leq 1.0$. Another emf measurement on the Mg–Sb system was carried out by Egan [28] at 1123 K in the composition range $0.1 \leq X_{Sb} \leq 0.9$. From the emf measurement, he determined the relative partial molar energy of Mg in liquid Mg–Sb alloys at 1123 K. The thermodynamic properties which were reported by both Rao and Patil [26] and Egan [28] are found to be in fair agreement. Also, Eremenko and Lukashenko [29] conducted an emf measurement in the temperature range 673–823 K. However, their values are found to be scattered. Vetter and Kubaschewski [30] measured the vapor pressure of Mg over liquid Mg–Sb alloys at 1133 and 1193 K in the composition range $0 \leq X_{Sb} \leq 0.66$. They measured the vapor pressure using a carrier gas entrainment method, and obtained the equilibrium pressure by extrapolation to zero flow rate. Their vapor pressure measurements are found to be unreliable beyond the composition of $X_{Sb} > 0.3$, as they neglected the Sb content in the vapor. Hence, the present work considers the reported thermodynamic properties of Vetter and Kubaschewski [30] in the composition range $0 < X_{Sb} < 0.3$ and that of Rao and Patil [26] in the composition range $0.3 < X_{Sb} < 1.0$. In addition, Eckert et al. [31] measured the thermodynamic activity of Mg in liquid Mg–Sb alloys at 1123 K across the whole concentration range using the emf technique. Their reported

Table 1
Crystal structure and lattice parameters of Mg_3Sb_2 [23]

Phase	Approximate composition[a] (at.% Sb)	Pearson symbol	Space group	Proto type	Lattice parameter (nm)	
					a	*c*
β-Mg_3Sb_2	40	cI 80	Ia3	βMn_2O_3	–	–
α-Mg_3Sb_2	40	hP 5	$P\bar{3}m_1$	La_2O_3	0.45822	0.72436

[a] From the phase diagram.

values are found to be in accord with Rao and Patil [26], and Vetter and Kubaschewski [30]. Hence, the present work considers their reported activity values too. Furthermore, Zabdyr and Moser [25] also employed an emf technique and reported activity coefficients of Mg in its dilute solution with Sb, and mentioned that their results were in good agreement with previously reported data.

Among available thermodynamic data on Mg_3Sb_2, much information is on the low temperature modification α-Mg_3Sb_2. The heat of formation of α-Mg_3Sb_2 relative to pure solid component was determined by several authors [26,29,32–35]. However, there is no such information available for β-Mg_3Sb_2 except the information on the heat capacity reported by Barin et al. [35] as $c_p = 160.7\,\mathrm{J/mol\,K}$.

2.2.3. Crystal structure data

Ganguli et al. [36] reported a single crystal investigation on α-Mg_3Sb_2. They reported that α-Mg_3Sb_2 is a classical example of a Zintl phase and was first studied by Zintl himself. The crystal structures and lattice parameters of α-Mg_3Sb_2 and β-Mg_3Sb_2 are summarized in Table 1.

2.3. The Mg–Al system

This system was thermodynamically modeled by several authors [37–42] and experimentally studied for new thermodynamic data by Moser et al. [43]. Moreover, Czeppe et al. [44], and Liang et al. [45] performed an experimental investigation in the central part of the Mg–Al phase diagram. In addition to the experimental investigation, Liang et al. [45] carried out thermodynamic calculations too.

The COST 507 project, which aimed at generating a thermochemical database for light metal alloys, was carried out by Ansara et al. [46]. In establishing the database for the Mg–Al system, they used the experimental investigation results from Liang et al. [45], and this database is found to be the most recent and reliable one for the Mg–Al system. The liquid phase in this database is constructed using the Redlich–Kister polynomial model; the pure elements have no added lattice stability values and the database is available. Therefore, the present research used this database for the Mg–Al binary system.

2.4. Mg–Al–Sb system

Guertler and Bergman [7] reported that in the quasi-binary Al–Mg_3Sb_2, the liquid miscibility gap extends from 9% to 98% mole fraction of Mg_3Sb_2. Loofs-Rassow [8] reported that the binary Al–AlSb, Al–Mg_3Sb_2, and AlSb–Mg_3Sb_2 exhibit binary or quasi-binary eutectics. They also found that Al–AlSb and AlSb–Mg_3Sb_2 are completely miscible in the liquid state while Al–Mg_3Sb_2 shows a miscibility gap. Later, the existence of this miscibility gap was supported by the experimental work of Guertler and Bergman [7].

3. Thermodynamic models

3.1. Unary phase

The Gibbs free energy of the pure element, i, with a certain structure, ϕ, at 298.15 K is described in terms of temperature as in Eq. (1):

$$ {}^{0}G_i^{\phi}(T) = a + bT + cT\ln T + dT^2 + eT^3 + fT^{-1} + gT^7 + hT^{-9} \quad (1) $$

where $a, b, \ldots, h$ are coefficients and the values are assigned from the SGTE database [47].

3.2. Disordered solution phase

The molar Gibbs free energy of the liquid phase in the Al–Sb and Mg–Sb systems is described using Eq. (2).

$$ G^{\mathrm{Liquid}} = X_i\,{}^{0}G_i^{\mathrm{Liquid}} + X_j\,{}^{0}G_j^{\mathrm{Liquid}} + RT[X_i\ln(X_i) + X_j\ln(X_j)] + {}^{\mathrm{ex}}G^{\mathrm{Liquid}} \quad (2) $$

where X_i and X_j represent the mole fraction of components i and j, respectively. The first two terms on the right-hand side of the equation represent the Gibbs free energy of the mechanical mixture of the components; the third term is the ideal Gibbs free energy of mixing; and the last term refers to the excess Gibbs free energy in the form of the Redlich–Kister polynomial equation, as in Eq. (3).

$$ {}^{\mathrm{ex}}G^{\mathrm{Liquid}} = X_iX_j\sum_{n=0}^{m}[{}^{n}L_{i,j}^{\mathrm{Liquid}}(X_i - X_j)^n] \quad (3) $$

and

$$ {}^{n}L_{i,j}^{\mathrm{Liquid}} = a_n + b_nT\ (n = 0, \ldots, m) \quad (4) $$

where a_n and b_n are model parameters to be optimized using experimental data.

3.3. Stoichiometric compound phase

AlSb is the only stoichiometric compound in the Al–Sb system. In the Mg–Sb system, the present work considers the low temperature modification of the intermediate phase, α-Mg_3Sb_2, as a line compound. The Gibbs free energy of these compounds is described using Eq. (5).

$$G^{\phi} = X_i\,{}^0G_i^{\phi_1} + X_j\,{}^0G_j^{\phi_2} + \Delta G_f \tag{5}$$

and

$$\Delta G_f = a + bT \tag{6}$$

where ϕ denotes the phase in question, ϕ_1 and ϕ_2 denote the reference structure of elements i and j, respectively, ${}^0G_i^{\phi_1}$ and ${}^0G_j^{\phi_2}$ represent the Gibbs free energy of components i and j in their standard states, respectively, ΔG_f represents the Gibbs free energy of formation of the stoichiometric compound, a and b are the model parameters to be optimized using experimental data.

3.4. Non-stoichiometric phase

In the Mg–Sb system, the present work considers β-Mg_3Sb_2 as a non-stoichiometric compound. However, there is no information available about the types of defects and the solubility range of β-Mg_3Sb_2. The only available information on this phase in the literature shows a very narrow solubility towards the Mg-rich side from the line of stoichiometry. The crystallographic data of β-Mg_3Sb_2 are not available. However, according to [23] the prototype of this phase is known to be β-Mn_2O_3. Crystal structure data of β-Mn_2O_3 are given in Table 2.

Table 2
Crystal structure data of β-Mn_2O_3 [48]

Atom	Atomic position (Wyckoff position)	X	Y	Z
Mn1	8b	0.25	0.25	0.25
Mn2	24d	0.97	0	0.25
O	48e	0.385	0.145	0.380

Space group number: 206.

According to the prototype of β-Mg_3Sb_2 the crystal structure analysis of this compound is carried out by replacing Mn with Sb and O with Mg, and the crystal structure of β-Mg_3Sb_2 is generated by PowderCell software [49]. A detailed look at the β-Mg_3Sb_2 crystal structure is shown in Fig. 1(a), (b) and (c).

From Fig. 1(a), (b) and (c) together with the Wyckoff position of Sb1, Sb2, and Mg atoms, the following can be deduced.

	Sb1	Sb2	Mg
The coordination number	12	12	15
Wyckoff position	8b	24d	48e
Mole fraction	0.1	0.3	0.6

According to Hari Kumar et al. [50] the atoms with the same coordination number can be combined and be considered as one sublattice. Hence, the sublattices of Sb1 and Sb2 are combined and considered as sublattice I with the mole fraction of 0.4. The Mg sublattice is named as sublattice II. Since the nature of the defects in the β-Mg_3Sb_2 is not known, the present study assumes that the substitutional atoms of Mg on Sb sites and Sb on Mg sites are the only defects. Hence, the species in the sublattices I and II are Mg and Sb. During the model parameter optimization of the β-Mg_3Sb_2, it was not possible to get the reported homogeneity range of this phase with two sublattices. Hence, 5/6th mole of the Mg sublattice is assumed to have defects. It is an arbitrary guess, and the remaining 1/6th mole is assumed without defects. In other words, the Mg sublattice is divided into two sublattices. They are:

(1) sublattice II with the mole fraction of 0.5 and with the species Mg and Sb;
(2) sublattice III with the mole fraction of 0.1 and with only Mg in it.

As the sublattice III is with pure Mg atoms, there is no mixing in this sublattice and the Gibbs free energy per mole of formula units can be written as in Eq. (7).

$$\begin{aligned} G_m = {} & y^{\mathrm{I}}_{\mathrm{Mg}} y^{\mathrm{II}}_{\mathrm{Mg}}\,{}^0G^{\mathrm{Mg_3Sb_2}}_{\mathrm{Mg:Mg:Mg}} + y^{\mathrm{I}}_{\mathrm{Mg}} y^{\mathrm{II}}_{\mathrm{Sb}}\,{}^0G^{\mathrm{Mg_3Sb_2}}_{\mathrm{Mg:Sb:Mg}} \\ & + y^{\mathrm{I}}_{\mathrm{Sb}} y^{\mathrm{II}}_{\mathrm{Mg}}\,{}^0G^{\mathrm{Mg_3Sb_2}}_{\mathrm{Sb:Mg:Mg}} + y^{\mathrm{I}}_{\mathrm{Sb}} y^{\mathrm{II}}_{\mathrm{Sb}}\,{}^0G^{\mathrm{Mg_3Sb_2}}_{\mathrm{Sb:Sb:Mg}} \\ & + RT\left(0.4\sum_{i=\mathrm{Mg}}^{\mathrm{Sb}} y^{\mathrm{I}}_i \ln y^{\mathrm{I}}_i + 0.5\sum_{i=\mathrm{Mg}}^{\mathrm{Sb}} y^{\mathrm{II}}_i \ln y^{\mathrm{II}}_i\right) \\ & + y^{\mathrm{II}}_{\mathrm{Mg}} y^{\mathrm{II}}_{\mathrm{Sb}}\,{}^0L^{\mathrm{Mg_3Sb_2}}_{\mathrm{Mg:Mg,Sb:Mg}} \end{aligned} \tag{7}$$

and

$$0.4\sum_{i=\mathrm{Mg}}^{\mathrm{Sb}} y^{\mathrm{I}}_i + 0.5\sum_{i=\mathrm{Mg}}^{\mathrm{Sb}} y^{\mathrm{II}}_i + 0.1 y^{\mathrm{III}}_{\mathrm{Mg}} = 1 \tag{8}$$

where $y^{\mathrm{I}}_{\mathrm{Mg}}, y^{\mathrm{II}}_{\mathrm{Mg}}, y^{\mathrm{III}}_{\mathrm{Mg}}$ are the site fractions of Mg in lattice I, II, and III respectively,

$y^{\mathrm{I}}_{\mathrm{Sb}}, y^{\mathrm{II}}_{\mathrm{Sb}}$ are the site fractions of Sb in lattice I and II respectively,

${}^0G^{\mathrm{Mg_3Sb_2}}_{\mathrm{Mg:Mg:Mg}}$, ${}^0G^{\mathrm{Mg_3Sb_2}}_{\mathrm{Mg:Sb:Mg}}$, ${}^0G^{\mathrm{Mg_3Sb_2}}_{\mathrm{Sb:Mg:Mg}}$, ${}^0G^{\mathrm{Mg_3Sb_2}}_{\mathrm{Sb:Sb:Mg}}$, and ${}^0L^{\mathrm{Mg_3Sb_2}}_{\mathrm{Mg:Mg,Sb:Mg}}$ are the parameters to be optimized using experimental data.

4. Results and discussion

4.1. Al–Sb binary system

The selected experimental phase diagram, enthalpy of mixing, entropy of mixing, Gibbs free energy of mixing and activities of liquid Al–Sb alloys data, which were discussed in Section 2.1, were used to optimize the thermodynamic

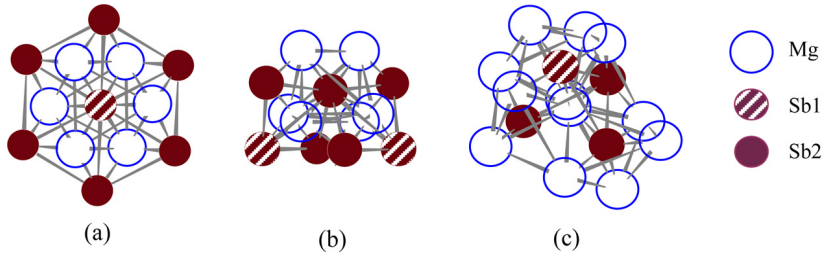

Fig. 1. Neighboring atoms around (a) Sb1, (b) Sb2, and (c) Mg.

model parameters of the liquid and AlSb phases. The optimization is done using the computer program WinPhaD Pro. [51]. The optimized model parameter values are given in Table 3.

Table 3
The optimized model parameters for the liquid and AlSb phases

Phase	Term	a (kJ/mol atom)	b (J/mol atom K)
Liquid	L_0	−13.328	−5.103
	L_1	10.748	0.337
AlSb	ΔG_f	−40.636	15.847

The reference structure of the Gibbs free energy of the formation of AlSb is considered as Al-fcc and Sb-rhombo. In order to maintain the consistency with other systems modeled by our group, no lattice stability values are added to the pure components Al-fcc and Sb-rhombo. From the optimized model parameters, the phase diagram of Al–Sb and the thermodynamic properties of Al–Sb system are calculated.

4.1.1. Phase diagram

The calculated phase diagram in relation to experimental data from the literature is shown in Fig. 2. Excellent agreement between the calculated phase diagram and measured liquidus points can be observed in this figure. It can be seen from Table 3 that only two Redlich–Kister terms (L_0 and L_1) were used to describe the liquid phase. A comparison between the current results and other works on this system is presented in Table 4.

4.1.2. Thermodynamic properties

As shown in Fig. 3(a), the calculated activities of Al and Sb in liquid Al–Sb alloys at 1350 K are in fair agreement with Zajaczkowski and Botor [14] and Predel and Schallner [18]. The calculated activity of Al shows slight positive deviation from the ideal behavior in the Al-rich side. Zajaczkowski and Botor [14] reported that this was the case in many other works too. In the Al-rich side, it can be observed that our calculated activity of Al lies in between Zajaczkowski and Botor [14] and Predel and Schallner [18]. However, the calculated values of Al in the Sb-rich side agree well with both Zajaczkowski and Botor [14] and

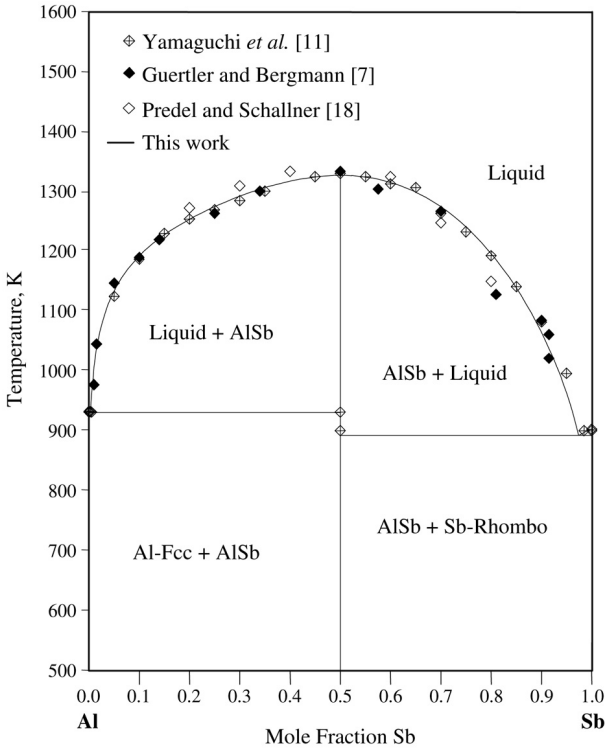

Fig. 2. Calculated Al–Sb phase diagram with experimental data from the literature.

Predel and Schallner [18]. The activity of Sb in liquid Al–Sb alloys shows negative deviation from ideal behavior in the whole range of composition. The calculated activity values of Sb from this work closely match with Zajaczkowski and Botor [14].

The calculated enthalpy of mixing of liquid Al–Sb alloys at 1350 K in Fig. 3(b) shows fairly good agreement with Yamaguchi et al. [11]. On the other hand the results of the current research agree with the enthalpy values reported by Batalin et al. [17] in the Al-rich side and deviate from those at the Sb-rich side.

The calculated entropy of mixing and Gibbs free energy of mixing of liquid Al–Sb alloys at 1350 K are shown in Fig. 3(c) and (d), respectively. As discussed in Section 2.1.2, the work of Yamaguchi et al. [11] is the only experimental data available for Gibbs free energy and entropy of mixing

Table 4
Comparison between different works (calculations) on the equilibria in the Al–Sb system

Reaction	Temp. (K)	Comp. (X_{Sb})	Solution model	Reference
L = (Al) + AlSb	931	–	Redlich–Kister polynomial	[10]
	928	–	Associated solution	[10]
	932	0.004	Redlich–Kister polynomial	[11]
	930.4	0.00476	Associated solution	[14]
	930	0.004	Associated solution	[9]
	931.3	0.0034	Redlich–Kister polynomial	This work
L = (Sb) + AlSb	897	–	Redlich–Kister polynomial	[10]
	897	–	Associated solution	[10]
	901	0.983	Redlich–Kister polynomial	[11]
	898.3	0.9833	Associated solution model	[14]
	899	0.984	Associated solution model	[9]
	893	0.974	Redlich–Kister polynomial model	This work
L = AlSb	1331	0.5	Redlich–Kister polynomial model	[10]
	1333	0.5	Associated solution model	[10]
	1335	0.5	Redlich–Kister polynomial model	[11]
	1336.4	0.5	Associated solution model	[14]
	1332	~0.5	Associated solution model	[9]
	1328.4	0.5	Redlich–Kister polynomial model	This work

of Al–Sb liquid. The results of the current work are in very good agreement with their results. It can be observed from Fig. 3(c) that, in the neighborhoods of $0.2 < X_{Sb} < 0.3$ and $0.55 < X_{Sb} < 0.75$, the calculated entropy of mixing of liquid Al–Sb shows some deviation from the values of Yamaguchi et al. [11]. Fig. 3(d) shows that, throughout the whole composition range, the calculated Gibbs free energy of mixing of Al–Sb liquid agrees with the experimental work of Yamaguchi et al. [11].

The calculated enthalpy and entropy of formation of the compound AlSb are compared with the reported literature data in Table 5.

Table 5
Calculated enthalpy and entropy of formation of AlSb with the reported data from the literature

Temperature (K)	ΔH_f (kJ/mol*)	ΔS_f (J/mol* K)	Reference
298	−96.60	−51.60	[21] Cal.
298	−73.49	−36.13	[10] Cal.
298	−84.00		[14] Cal.
298	−82.00 ± 2.51		[15] Exp.
298	−81.27	−42.13	This work

mol* = mole of formula units; Cal. denotes calculated values by associated solution model; Exp. denotes experimental value by drop calorimetry.

Table 5 shows that the calculated enthalpy and entropy of formation of AlSb in the present research is in good agreement with the calculated and experimental results reported in the literature.

4.2. Mg–Sb binary system

The selected experimental data of the phase diagram, enthalpy of mixing, entropy of mixing, Gibbs free energy of mixing and activities of components Mg and Sb in liquid Mg–Sb alloys, which were discussed in Section 2.2, were used to optimize the thermodynamic model parameters for the liquid, α-Mg_3Sb_2, and β-Mg_3Sb_2 phases. The optimized model parameters for the liquid, α-Mg_3Sb_2, β-Mg_3Sb_2 are given in Table 6.

Table 6
The optimized parameters for the liquid, α-Mg_3Sb_2, and β-Mg_3Sb_2

Phase	Term	a (J/mol atom)	b (J/mol atom K)
Liquid	L_0	−172 660.521	44.865
	L_1	−157 139.842	123.000
	L_2	29 500.000	10.637
	L_3	127 386.016	−98.780
α-Mg_3Sb_2	ΔG_f	−98 006.025	48.795
β-Mg_3Sb_2	G(Mg:Mg:Mg)	65 000.000	
	G(Mg:Sb:Mg)	−37 429.535	−2.010
	G(Sb:Sb:Mg)	39 651.000	−9.048
	L(Mg:Mg, Sb:Mg)	−150 000.000	60.000

The reference structure of the Gibbs free energy of formation of α-Mg_3Sb_2 is considered as Mg-hcp and Sb-rhombo. No lattice stability values are added to the pure components Mg-hcp and Sb-rhombo. From the optimized model parameters, the phase diagram and the thermodynamic properties of the Mg–Sb system

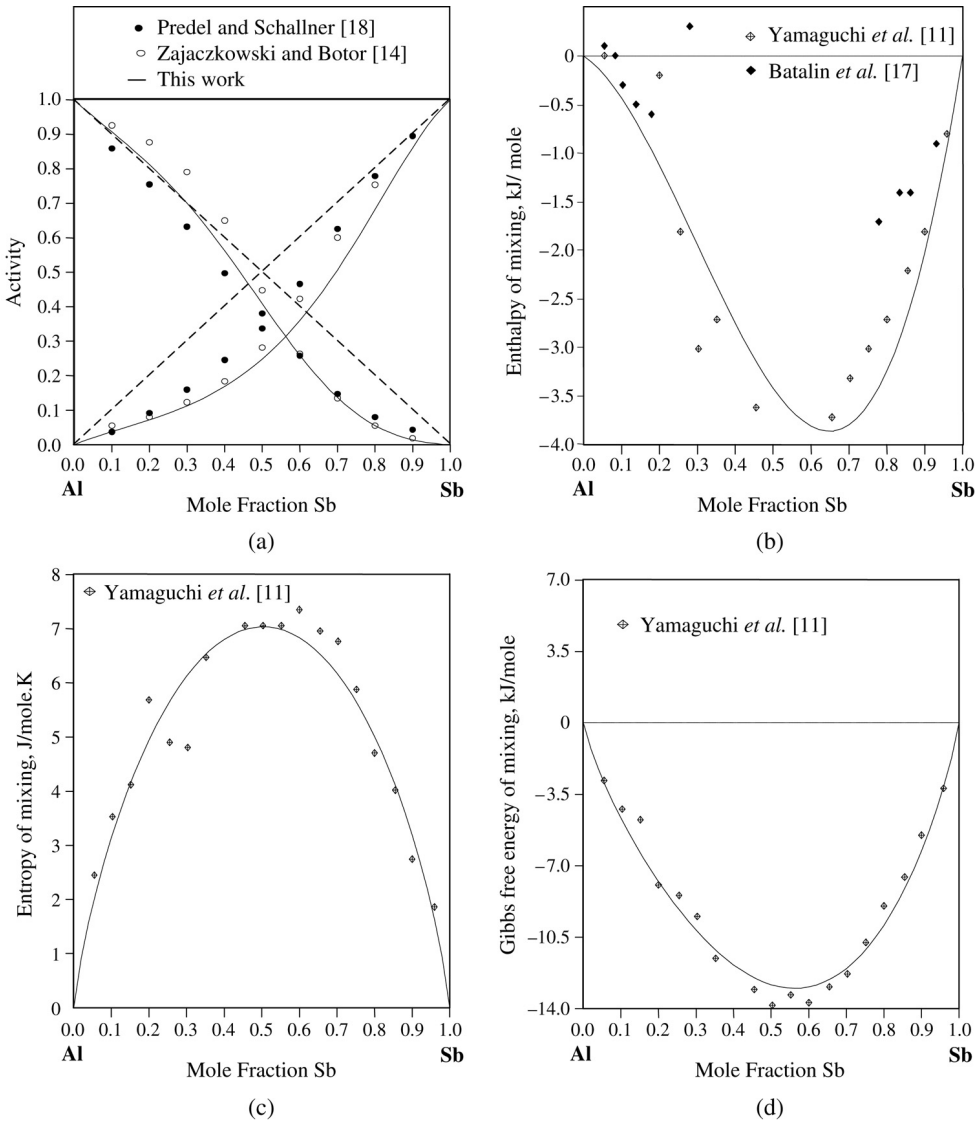

Fig. 3. Calculated (a) activities, (b) enthalpy of mixing, (c) entropy of mixing, (d) Gibbs free energy of mixing of liquid Al–Sb alloys at 1350 K in relation to experimental data from the literature.

are calculated. Moreover, the obtained database can be combined with other binaries and used to interpolate and extrapolate the thermodynamic properties as well as to calculate meta-stable phase boundaries.

4.2.1. Phase diagram

The calculated phase diagram is shown in Fig. 4. It shows a fair agreement with the experimental data of Grube [19], Grube and Bornhak [20], Hansen and Anderko [22], and Rao and Patil [26]. A comparison between the results of the critical points obtained in the current research is given in Table 7.

4.2.2. Thermodynamic properties

The calculated thermodynamic properties are in good agreement with the experimental data reported in the literature. As shown in Fig. 5(a), the calculated activity of Mg in liquid Mg–Sb alloys at 1073 K is in fairly good agreement with the experimental data of Rao and Patil [26] and Eckert et al. [31].

The calculated entropy of mixing of liquid Mg–Sb alloys at 1073 K, Fig. 5(b), shows very good agreement with the experimental data of Rao and Patil [26]. It can be observed from Fig. 5(b) that, in the composition range $0.2 < X_{Sb} < 0.4$, the liquid Mg–Sb alloys show minimum (−ve) entropy, and in the range $0.7 < X_{Sb} < 0.85$ they show maximum (+ve) entropy. That is, within the composition range $0.2 < X_{Sb} < 0.4$, the liquid is relatively ordered and in the range $0.7 < X_{Sb} < 0.85$ it is highly disordered.

The calculated enthalpy of mixing and Gibbs free energy of mixing of liquid Mg–Sb at 1073 K are shown in Fig. 5(c) and (d), respectively. They also show good agreement with the experimental data from the literature.

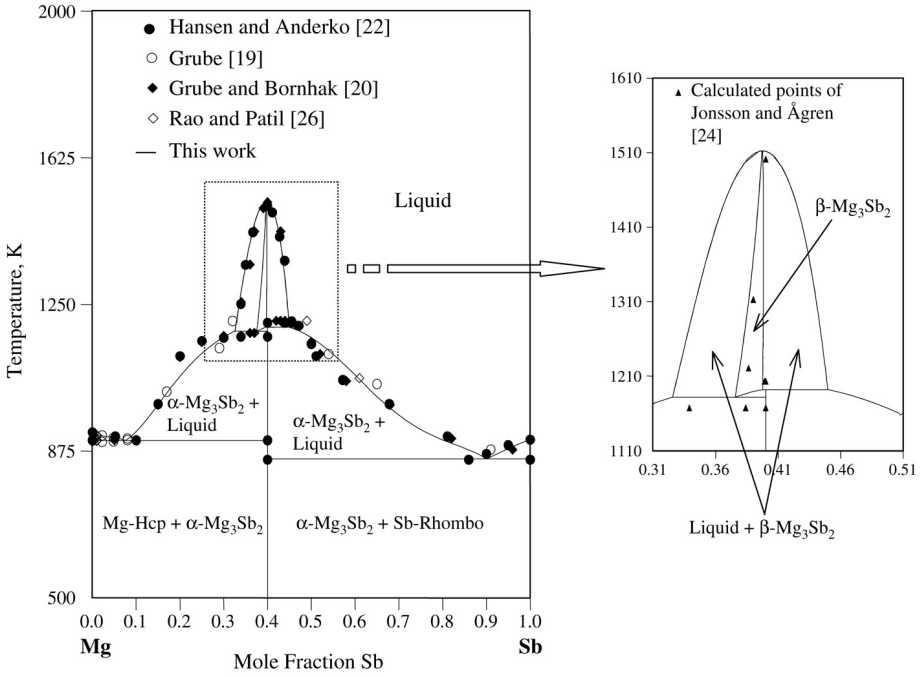

Fig. 4. Calculated Mg–Sb phase diagram with experimental data from the literature.

Table 7
Comparison between different works (calculations) on the equilibria in the Mg–Sb system

Reaction	Temperature (K)	Composition (X_{Sb})	Reference
$L = (Mg) + \alpha\text{-}Mg_3Sb_2$	902	0.026	[24]
	902	0.1	[20]
	902	0.1	[22]
	902	0.1	[29]
	902	0.076	This work
$L = (Sb) + \alpha\text{-}Mg_3Sb_2$	852	0.848	[24]
	852	0.86	[20]
	852	0.86	[22]
	852	∼0.87	[29]
	854	0.9	This work

Table 8
Calculated enthalpy and entropy of formation of α-Mg_3Sb_2 with the reported data from the literature

Temperature (K)	ΔH_f (kJ/mol*)	ΔS_f (J/mol* K)	Reference
900	-299 ± 3	-59 ± 5	[26] Exp. 1
773	-235 ± 6	-15 ± 10	[29] Exp. 1
923	-285		[32] Exp. 2
800	-320 ± 40	-91 ± 52	[34] Cal.
298	-300		[35] Cal.
298	-490	-54	This work

mol* = mole of formula units; Exp. 1 denotes the experimental values by emf measurements; Exp. 2 denotes the experimental value by high temperature calorimetric measurements; Cal. denotes calculated values.

The calculated enthalpy and entropy of formation of the compound α-Mg_3Sb_2 are compared with the data reported in the literature in Table 8.

It can be observed from Table 8 that the calculated enthalpy value in the present research is higher than the experimental values reported in the literature. This may be due to the assumption that the low temperature modification α-Mg_3Sb_2 is a stoichiometric compound.

4.3. Mg–Al–Sb ternary system

For the first time the Mg–Al–Sb system is thermodynamically modeled. A database was constructed for this system by combining the binary thermodynamic descriptions of Mg–Al, Al–Sb, and Mg–Sb. The database is used to calculate polythermal projections of liquidus surfaces.

A two-dimensional representation of the ternary liquidus surface is obtained as an orthogonal projection upon the base composition triangle with components Mg, Al, and Sb and shown in Fig. 6. There is a closed ternary liquid miscibility gap in the composition range $0.0048 < X_{Sb} < 0.375$.

The characteristic points in the Mg–Al–Sb ternary phase diagram are

(1) 6 ternary eutectics: E_1, E_2, E_3, E_4, E_5, and E_6;
(2) 4 saddle points: S_1, S_2, S_3, and S_4;
(3) 2 ternary quasi-peritectic points: P_1, and P_2;
(4) 1 critical point.

Table 9 shows the estimated characteristic points and expected reactions at those points.

The obtained thermodynamic database for the Mg–Al–Sb system is used to predict the pseudo-binary diagram of

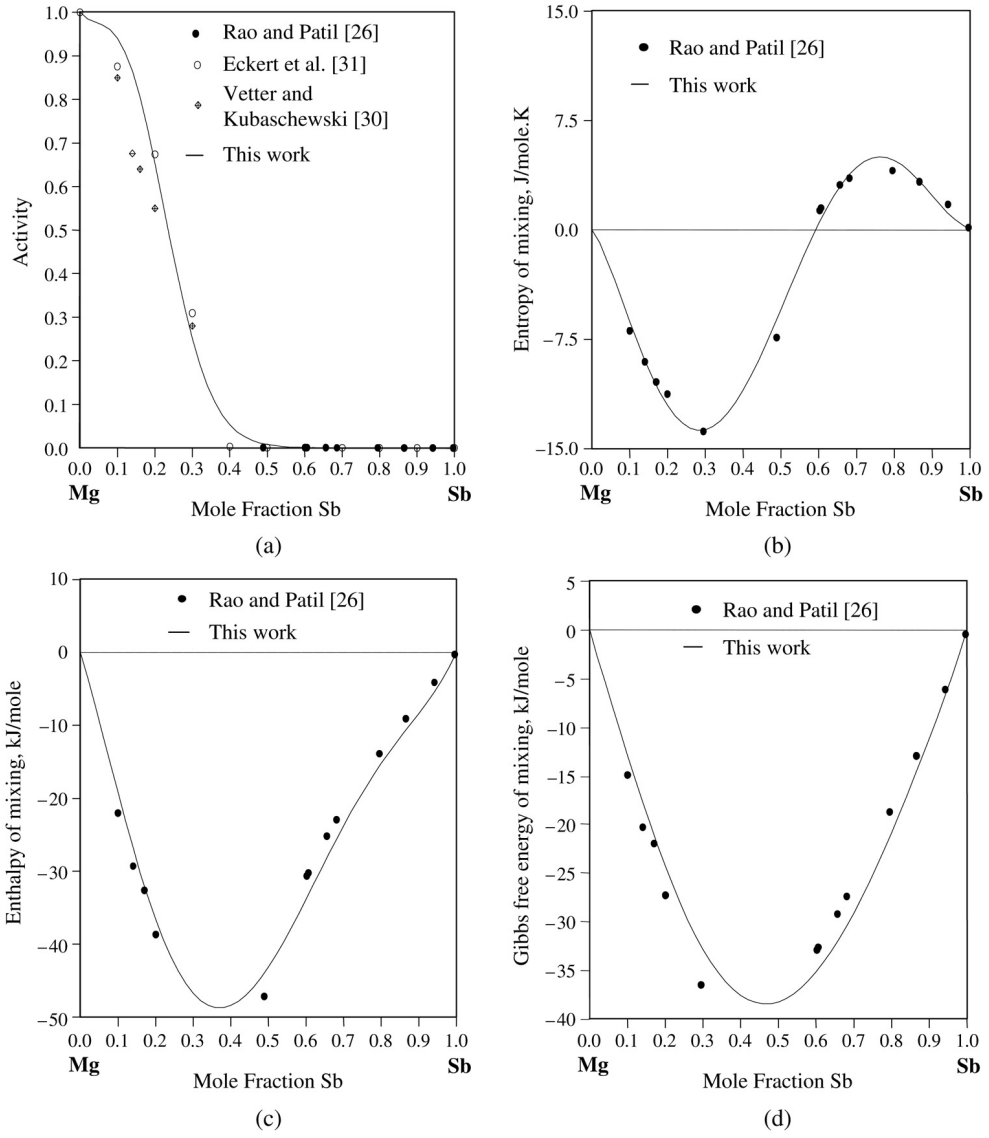

Fig. 5. Calculated (a) activity of Mg, (b) entropy of mixing, (c) enthalpy of mixing, (d) Gibbs free energy of mixing of liquid Mg–Sb alloys at 1073 K in relation to experimental data from the literature.

Table 9
Calculated characteristic points and reactions

Critical point	X_{Sb}	X_{Mg}	Temperature (K)	Reaction
E_1	0.902	0.093	852.6	$L \leftrightarrow AlSb + Sb + \alpha\text{-}Mg_3Sb_2$
E_2	0.063	0.930	898.8	$L \leftrightarrow \alpha\text{-}Mg_3Sb_2 + (Mg)$
E_3	0.1E–7	0.690	708.9	$L \leftrightarrow (Mg) + \alpha\text{-}Mg_3Sb_2 + \gamma$
E_4	0.1E–7	0.424	721.8	$L \leftrightarrow \gamma + \alpha\text{-}Mg_3Sb_2 + Al_{140}Mg_{89}$
E_5	0.1E–7	0.362	723.4	$L \leftrightarrow \alpha\text{-}Mg_3Sb_2 + (Al) + Al_{140}Mg_{89}$
E_6	0.003	0.002	930.2	$L \leftrightarrow AlSb + (Al) + \alpha\text{-}Mg_3Sb_2$
S_1	0.430	0.398	1136.9	$L \leftrightarrow \alpha\text{-}Mg_3Sb_2 + AlSb$
S_2	0.292	0.472	1164.0	$L/L_1 + \alpha\text{-}Mg_3Sb_2$
S_3	0.037	0.950	901.0	$L \leftrightarrow Mg_3Sb_2 + (Mg)$
S_4	0.278	0.121	1226.0	$L/L_1 + AlSb$
P_1	0.075	0.040	1133.23	$L/L_1 + \alpha\text{-}Mg_3Sb_2 + AlSb$
P_2	0.017	0.959	897.38	$L/L_1 + \alpha\text{-}Mg_3Sb_2 + (Mg)$
Critical point	0.100	0.506	1383.70	$L \leftrightarrow L_1 + L_2$

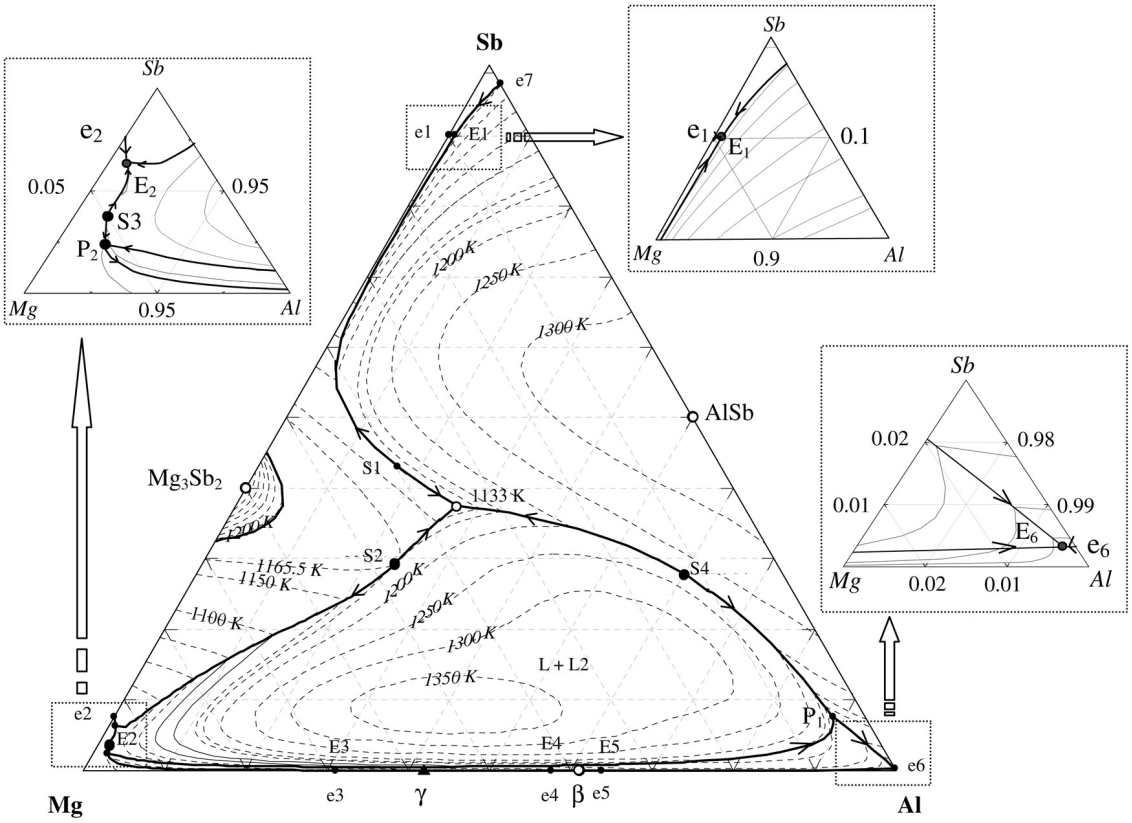

Fig. 6. Projection of the liquidus surface of the Mg–Al–Sb system onto a ternary composition triangle.

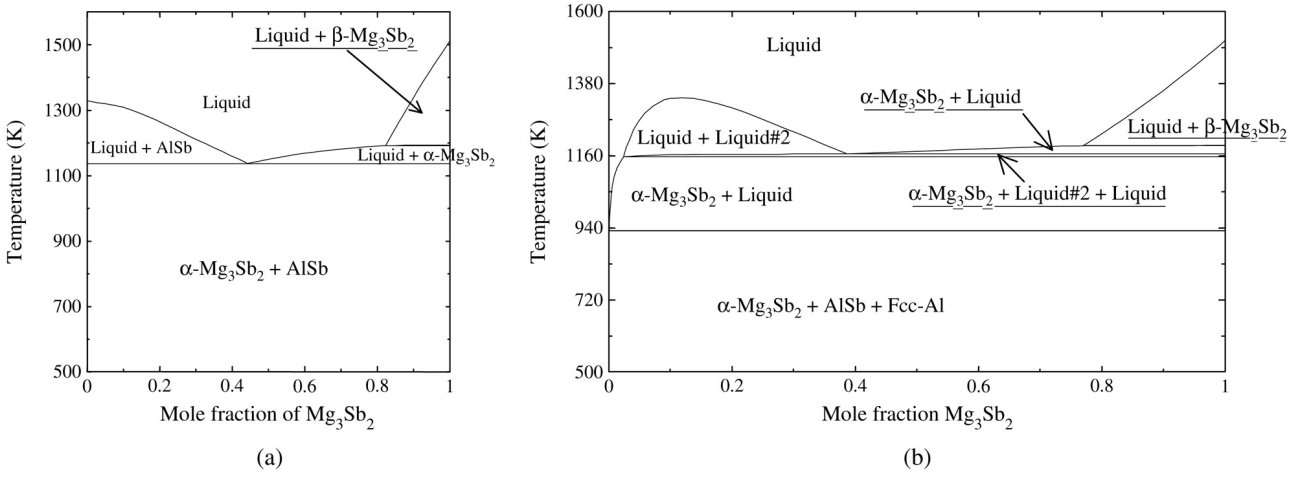

Fig. 7. (a) Calculated AlSb–Mg_3Sb_2 pseudo-binary phase diagrams. (b) Calculated Al–Mg_3Sb_2 isopleth.

AlSb–Mg_3Sb_2, and the isopleth diagram of Al–Mg_3Sb_2. These diagrams are shown in Fig. 7 and will be compared with the reported experimental observations from the literature [7,8].

Both Fig. 7(a) and (b) do not show a liquid miscibility gap; this is supported by the experimental work of Loofs-Rassow [8]. Moreover, Loofs-Rassow [8] and Guertler and Bergman [7] reported that there is a liquid miscibility gap in the binary Al–Mg_3Sb_2. This experimental observation was also reproduced in the isopleth Al–Mg_3Sb_2 calculated from the current thermodynamic model and shown in Fig. 7(c).

5. Conclusions

In this research, the Mg–Al–Sb system was thermodynamically modeled and the following conclusions were drawn.

Optimized thermodynamic model parameters for different phases in the binaries Al–Sb, and Mg–Sb were obtained, where the liquid phases were described by the Redlich–Kister polynomial model and the non-stoichiometric compound β-Mg_3Sb_2 was described by a sublattice model. The model parameters of different phases were optimized with no added lattice stability values to the pure components Mg-hcp, Al-fcc, and Sb-rhombo.

From the obtained optimized model parameters, phase diagrams of Al–Sb, Mg–Sb and the thermodynamic properties such as enthalpy, entropy, Gibbs free energy, and activity were calculated and compared with the experimental literature data. The calculated phase diagrams and thermodynamic properties were found to be in good agreement with the data reported in the literature.

The thermodynamic database of the Mg–Al–Sb system was constructed by combining the databases of the constituent binaries Mg–Al, Al–Sb, and Mg–Sb. From the established thermodynamic database, the Mg–Al–Sb ternary phase diagram was calculated and the characteristic points were predicted. It was found that the Mg–Al–Sb system has six eutectics, four saddle points, two P-type invariant points, and a critical point.

A closed ternary liquid miscibility gap was predicted by the established Mg–Al–Sb thermodynamic database and found to be consistent with the reported experimental observations in the literature.

Acknowledgements

The authors gratefully acknowledge the financial support from NSERC, Canada through the Discovery Grant Program and NATEQ, Quebec, Canada through Èstablissement de Nouveaux chercheurs program.

References

[1] C.J. Bettles, P. Humble, J.F. Nie, Proceedings of the 3rd International Magnesium Conference, 1996, p. 403–417.
[2] E.F. Emley, Principles of Magnesium Technology, Pergamon Press, London, 1966, p. 879.
[3] G.V. Raynor, The Physical Metallurgy of Magnesium and Its Alloys, Pergamon Press, London, 1959, p. 386.
[4] C.S. Robers, Magnesium and Its Alloys, John Weily and Sons Inc., New York, 1960, p. 101.
[5] Y. Guangyin, S. Yangshan, D. Wenjiang, Scr. Mater. 43 (2000) 1009–1013.
[6] W. Guertler, A. Bergmann, Z. Metallkunde 25 (1933) 81–84.
[7] W. Guertler, A. Bergmann, Z. Metallkunde 25 (1933) 111–116.
[8] E. Loofs-Rassow, Hauszeitschrift, V.A.W. Erftwerk A.G., Aluminium 3 (1931) 20–32.
[9] K. Yamaguchi, K. Itagaki, Y.A. Chang, CALPHAD 20 (1996) 439–446.
[10] C.A. Coughanowr, U.R. Kattner, T.J. Anderson, CALPHAD 14 (1990) 193–202.
[11] K. Yamaguchi, M. Yoshizawa, Y. Takeda, K. Kameda, K. Itagaki, Mater. Trans. JIM 36 (1995) 432–437.
[12] R. Linnebach, K.W. Benz, J. Cryst. Growth 55 (1981) 531–538.
[13] H. Okamoto, J. Phase Equilib. 12 (1991) 623–643.
[14] A. Zajaczkowski, J. Botor, Z. Metallkunde 86 (1995) 590–596.
[15] B.D. Lichter, P. Sommelet, Trans. Metall. Soc. AIME 245 (1969) 99–105.
[16] C. Girard, J.M. Miane, J. Riou, R. Baret, J.P. Bros, J. Less-Common Met. 128 (1987) 101–115.
[17] G.I. Batalin, V.E. Sokol'skii, T.B. Shimanskaya, Ukr. Khim. Zh. 37 (1971) 397.
[18] B. Predel, U. Schallner, Mater. Sci. Eng. 5 (1970) 210–219.
[19] G. Grube, Z. Anorg. Chem. 49 (1906) 87–91.
[20] G. Grube, R. Bornhak, Z. Elektrochem. 40 (1934) 140–142.
[21] W.R.D. Jones, L. Powell, J. Inst. Met. 67 (1941) 177–188.
[22] M. Hansen, K. Anderko, in: R.F. Mehl, M.B. Bever (Eds.), Constitution on Binary Alloys, McGraw-Hill, NY, 1958, pp. 915–916.
[23] A.A. Nayeb-Hashemi, J.B. Clark, Bull. Alloy Phase Diag. 5 (1985) 579–584.
[24] B. Jönsson, J. Ågren, Metall. Trans. 18 (1987) 1395–1401.
[25] L. Zabdyr, Z. Moser, Bull. Pol. Acad. Sci. Tech. Sci. 31 (1983) 37–42.
[26] Y.K. Rao, B.V. Patil, Metall. Trans. 2 (1971) 1829–1835.
[27] K.A. Bolshakov, N.A. Bulonkov, M.S. Tsirlin, Zh. Neorg. Khim.; Russ. J. Inorg. Chem. (Engl. Transl.) 7 (1962) 1176.
[28] J.J. Egan, J. Nucl. Mat. 51 (1974) 30–35.
[29] V.N. Eremenko, G.M. Lukashenko, Zh. Neorg. Khim.; Russ. J. Inorg. Chem. (Engl. Transl.) 9 (1964) 1552–1555.
[30] F.A. Vetter, O. Kubaschewski, Z. Elektrochem. 57 (1953) 243–248.
[31] C.A. Eckert, R.B. Irwin, J.S. Smith, Metall. Trans. 14 (1983) 451–458.
[32] O. Kubaschewski, A. Walter, Z. Elektrochem. 45 (1939) 732–740.
[33] O. Kubaschewski, J.A. Catterall, Thermodynamic Data of Alloys, Pergamon Press, New York, 1956.
[34] R. Hultgren, P.D. Desai, D.T. Hawkins, M. Gleiser, K.K. Kelley, Selected Values of the Thermodynamic Properties of Binary Alloys, ASM International, Metals Park, OH, 1973, pp. 1106–1108.
[35] I. Barin, O. Knacke, O. Kubaschewski, Thermochemical Properties of Inorganic Substances, Supplement, Springer-Verlag, 1977, p. 385.
[36] A.K. Ganguli, Y.U. Kwon, J.D. Corbett, Inorg. Chem. 32 (1993) 4354–4359.
[37] J.L. Murray, Bull. Alloy Phase Diag. 3 (1982) 60–74.
[38] M.L. Saboungi, C.C. Hsu, Applications of Phase Diagrams in Metallurgy and Ceramics Proceedings of Workshop, Gaithersburg, 1977, pp. 1109–1138.
[39] D. Ludecke, K. Hack, Z. Metallkunde 77 (1986) 145–161.
[40] N. Saunders, CALPHAD 14 (1990) 61–70.
[41] Y. Zuo, Y.A. Chang, CALPHAD 17 (1993) 161–174.
[42] P. Chartrand, A.D. Pelton, J. Phase Equilib. 15 (1994) 591–605.
[43] Z. Moser, W. Zakulski, W. Gasior, Z. Panek, I. Matsuda, Y. Fukuda, T. Iida, Z. Zajaczkowski, J. Botor, J. Phase Equilib. 19 (1998) 38–45.
[44] T. Czeppe, W. Zakulski, E. Bielanska, J. Phase Equilib. 4 (2003) 249–254.

[45] P. Liang, H.L. Su, P. Donnadieu, M. Harmelin, A. Quivy, Z. Metallkunde 89 (1998) 536–540.
[46] I. Ansara, A.T. Dinsdale, M.H. Rand, COST 507—Thermochemical Database for Light Metal Alloys, European Commission EUR 18499, 1998.
[47] A.T. Dinsdale, CALPHAD 15 (1991) 317–425.
[48] T. Hahn, International Tables for Crystallography, Volume A—Space Group Symmetry, 3rd edition, Kluwer Academic Publishers, 1992.
[49] PowderCell, Programmed by W. Kraus, and G. Nolze, BAM Berlin.
[50] K.C. Hari Kumar, I. Ansara, P. Wollants, CALPHAD 22 (1998) 323–334.
[51] WinPhaD 2.0—Phase Diagram Calculation Engine for Binary Systems, CompuTherm LLC, Madison, WI, USA, 2000.